J|A|C|S
ARTICLES

Published on Web 07/27/2010

Mechanism for Recognition of Polyubiquitin Chains: Balancing Affinity through Interplay between Multivalent Binding and Dynamics

Craig J. Markin,[†] Wei Xiao,[‡] and Leo Spyracopoulos*,[†]

Department of Biochemistry, School of Molecular and Systems Medicine, University of Alberta, Edmonton, Alberta T6G 2H7, Canada, and Department of Microbiology and Immunology, University of Saskatchewan, Saskatoon, Saskatchewan S7N 5E5, Canada

Received May 6, 2010; E-mail: leo.spyracopoulos@ualberta.ca

Abstract: RAP80 plays a key role in signal transduction in the DNA damage response by recruiting proteins to DNA damage foci by binding K63-polyubiquitin chains with two tandem ubiquitin-interacting motifs (tUIM). It is generally recognized that the typically weak interaction between ubiquitin (Ub) and various recognition motifs is intensified by themes such as tandem recognition motifs and Ub polymerization to achieve biological relevance. However, it remains an intricate problem to develop a detailed molecular mechanism to describe the process that leads to amplification of the Ub signal. A battery of solution-state NMR methods and molecular dynamics simulations were used to demonstrate that RAP80-tUIM employs mono- and multivalent interactions with polyUb chains to achieve enhanced affinity in comparison to monoUb interactions for signal amplification. The enhanced affinity is balanced by unfavorable entropic effects that include partial quenching of rapid reorientation between individual UIM domains and individual Ub domains in the bound state. For the RAP80-tUIM−polyUb interaction, increases in affinity with increasing chain length are a result of increased numbers of mono- and multivalent binding sites in the longer polyUb chains. The mono- and multivalent interactions are characterized by intrinsically weak binding and fast off-rates; these weak interactions with fast kinetics may be an important factor underlying the transient nature of protein−protein interactions that comprise DNA damage foci.

Introduction

The covalent attachment of ubiquitin (Ub) to target proteins is crucial to the regulation of life processes such as protein degradation, the cell cycle, DNA repair, the DNA damage response, and trafficking.[1] Ultimately, manifestation of the Ub signal on target proteins may be attachment of a single or multiple Ub molecules to different sites or polyubiquitination through a single type or varied intra-Ub peptide linkages. These various forms of the Ub signal provide a topological richness that can be exploited to achieve specificity in a wide variety of signaling cascades, as typified by the diversity in Ub recognition by domains such as UIM, UEV, CUE, and LUBAC.[2] Some of these domains consist of well-structured cores, whereas others, such as the ubiquitin-interacting motif (UIM), consist of single or tandem α-helices. Invariably, recognition of the mono-Ub signal by a single Ub binding domain occurs with weak affinity, having a typical dissociation constant exceeding 100 μM.[3] While there are numerous examples that the basic monoUb interaction is intensified by themes such as tandem Ub recognition motifs to achieve biological relevance, it remains a difficult and intricate problem to develop a detailed molecular mechanism to describe the process that leads to amplification of the Ub signal.

Recently, K63-linked polyUb chain recognition has been implicated in the DNA damage response (DDR) through its involvement in the repair of double-stranded DNA breaks (DSB).[4−6] The DDR involves a cascade of altered proteins and protein−protein interactions in response to damaged DNA;[7] the process has been likened to signal transduction networks.[8] The protein RAP80 has been shown to play a key role in the DDR by recruiting proteins critical for repair to DNA damage foci via recognition of polyUb chains through tandem ubiquitin-interacting motifs (tUIMs) at its N-terminus.[4−6] A breakdown in protein targeting to DNA damage foci can lead to tumorigenesis.[6] For example, BRCA1 (breast cancer 1, early onset protein) is a tumor suppressor that is mutated in about half of all hereditary early-onset breast and ovarian cancer patients,[5] and its recruitment to sites of DNA damage is critical for repair.

RAP80 is a ∼80 kDa multidomain protein consisting of two putative zinc fingers and two tandem ubiquitin interacting motifs (UIMs). Canonical UIMs consist of a single short α-helix that

[†] University of Alberta.
[‡] University of Saskatchewan.

(1) Komander, D. *Biochem. Soc. Trans.* **2009**, *37*, 937–953.
(2) Dikic, I.; Wakatsuki, S.; Walters, K. J. *Nat. Rev. Mol. Cell. Biol.* **2009**, *10*, 659–671.
(3) Hurley, J. H.; Lee, S.; Prag, G. *Biochem. J.* **2006**, *399*, 361–372.
(4) Wang, B.; Matsuoka, S.; Ballif, B. A.; Zhang, D.; Smogorzewska, A.; Gygi, S. P.; Elledge, S. J. *Science* **2007**, *316*, 1194–1198.
(5) Kim, H.; Chen, J. J.; Yu, X. H. *Science* **2007**, *316*, 1202–1205.
(6) Sobhian, B.; Shao, G. Z.; Lilli, D. R.; Culhane, A. C.; Moreau, L. A.; Xia, B.; Livingston, D. M.; Greenberg, R. A. *Science* **2007**, *316*, 1198–1202.
(7) Matsuoka, S.; Ballif, B. A.; Smogorzewska, A.; McDonald, E. R.; Hurov, K. E.; Luo, J.; Bakalarski, C. E.; Zhao, Z. M.; Solimini, N.; Lerenthal, Y.; Shiloh, Y.; Gygi, S. P.; Elledge, S. J. *Science* **2007**, *316*, 1160–1166.
(8) Petrini, J. H. J. *Science* **2007**, *316*, 1138–1139.

interacts with the I44 hydrophobic patch on Ub with low affinity ($K_D \sim 0.1-2$ mM). The canonical α-helical UIM binds Ub in a specific fashion, such that the N-terminus of the UIM is adjacent to the C-terminus of Ub and the C-terminus of the UIM is adjacent to the N-terminus (or K63) of Ub.[9] Recently, the interaction of RAP80-tUIM with K63-linked Ub_2 and Ub_4 chains was characterized by isothermal titration calorimetry and fluorescence anisotropy measurements,[10] and the structure of the complex was determined by crystallography.[11] It was shown that binding of Ub_2 to the tandem RAP80 UIMs is enhanced compared to binding of monoUb, and similarly, binding of Ub_4 is enhanced in comparison to Ub_2. In addition, the length of the linker between the tandem UIMs of RAP80 was shown to influence the affinity of the Ub_2−RAP80-tUIM interaction. Herein, we have used solution-state NMR spectroscopy in combination with molecular dynamics simulations to demonstrate that recognition of extended, tandemly linked polyUb molecules by the tandem UIM domains of RAP80 occurs through interplay between multivalent binding of sequential UIMs to sequential Ub moieties and dynamics between the individual domains. Tandem, or linear, polyUb chains are composed of Ub domains linked sequentially through their respective N- and C-termini. These polyUb chains serve biological roles and, given their close structural and dynamic similarity to K63-linked chains, can also serve as models for understanding recognition processes for K63-linked chains. Importantly, we have developed a basic multivalent binding model for the interaction of RAP80-tUIM with tandem polyUb chains that accounts for the Ub chain length dependence of the affinity of the interaction. Furthermore, we observe fast kinetics for the interaction of tandem Ub_2 with RAP80-tUIM that may be physiologically relevant for maintaining transient protein complexes at DNA damage foci. We also show that conformational selection plays an important role in UIM−polyUb recognition through analysis of the temperature dependence of main-chain $^{13}C_\alpha$ and $^1H_\alpha$ chemical shifts and ^{15}N NMR relaxation measurements of the main-chain dynamics for RAP80-tUIM.

Materials and Methods

Protein Expression and Purification. All proteins were cloned and expressed as pGEX6P-1 glutathione S-transferase (GST) fusion constructs in *Escherichia coli* BL21DE3 cells. Protein sequences are given in the Supporting Information. For expression of the isotopically labeled RAP80-tUIM and polyUb proteins, cells were grown as previously described.[12] For unlabeled proteins, the methodology was as follows: Electrocompetent cells were transformed and plated on agar plates containing ampicillin and chloramphenicol overnight. A single colony was used to inoculate starter cultures of 50 mL of Luria broth (LB) with antibiotics added and allowed to grow overnight. Four flasks of 500 mL of LB were then inoculated with 5 mL of starter culture, grown to OD_{600} of ∼0.6−0.8, and induced with 1.6 mL of 125 mM isopropyl thiogalactoside (IPTG). Expression was allowed to proceed overnight at 18 °C for RAP80-tUIM or at 25 °C for tandem polyUb chains.

Purification methods for the various proteins used in this study were similar except where noted. After harvesting and lysing of cells, the lysate was passed over a GST affinity column. The ubiquitin constructs were cleaved by use of PreScission protease enzyme in 50 mM tris(hydroxymethyl)aminomethane (Tris) and 200 mM NaCl buffer, pH 7.0. GST−RAP80-tUIM was cleaved in 50 mM Tris and 150 mM NaCl buffer, pH 7.5. Following cleavage, protein solutions were passed over a GST affinity column, followed by size-exclusion chromatography to purify RAP80-tUIM and Ub (Superdex 30) and Ub_2 and Ub_4 (Superdex 75). For Ub_3, ion-exchange purification via a Q-Sepharose column was employed, followed by size-exclusion chromatography on a Superdex 75 column.

NMR Spectroscopy. The majority of NMR spectra were collected at 25 °C and 600 MHz, with the exception of the titration of [U-^{15}N, U-^{2}H]RAP80-tUIM with unlabeled Ub_4, which was carried out at 800 MHz. NMR titrations of unlabeled monoUb, tandem Ub_2, tandem Ub_3, and tandem Ub_4 into [U-^{15}N]RAP80-tUIM (Ub_3) or [U-^{15}N, U-^{2}H]RAP80-tUIM (Ub, Ub_2, Ub_4) were conducted by following chemical shift changes for backbone amide $^1H^N$ and ^{15}N resonances in 2D $^1H-^{15}N$ heteronuclear single quantum coherence (HSQC) or transverse relaxation-optimized spectroscopy (TROSY) HSQC NMR spectra. In order to ensure consistency of the results, corollary titrations of [U-^{15}N]Ub_2, [U-^{15}N]Ub_3, and [U-^{15}N, U-^{2}H]Ub_4 with unlabeled RAP80-tUIM were conducted in a similar manner. For the 2D $^1H-^{15}N$ HSQC NMR-based titrations, samples initially contained labeled protein in a 95:5 H_2O/D_2O mixture, containing 50 mM Tris, 150 mM NaCl, and 1 mM dithiothreitol (DTT) (pH 7.3). To this mixture, a stock solution of unlabeled binding partner in the same buffer conditions was added to follow chemical shift changes.

For relaxation experiments, 350 μL samples of [U-^{15}N]/[U-^{13}C, U-^{15}N]-labeled RAP80-tUIM were placed in 5 mm Shigemi tubes in either 95:5 H_2O/D_2O or 90:10 H_2O/D_2O containing 50 mM Tris, 150 mM NaCl, 1 mM DTT, and 0.5 μL of 10% NaN_3. [U-^{13}C, U-^{15}N]-labeled samples used for chemical shift assignment were prepared similarly, with the inclusion of 5 μL of 10 mM DSS as a chemical shift reference. Chemical shift assignments were accomplished by standard $^1H/^{13}C/^{15}N$ protein NMR spectroscopy.[13]

1:1 Binding Isotherms for RAP80-tUIM Interactions with Tandem Ub_2, Ub_3, and Ub_4. As a first step in analyzing the binding of RAP80-tUIM to polyUb, macroscopic K_D values were determined for each individual titration of unlabeled tandem Ub_2, Ub_3, and Ub_4 into [U-^{15}N]- or [U-^{15}N, U-^{2}H]RAP80-tUIM by globally fitting titration data for all residues observed to shift significantly with a basic binding isotherm describing 1:1 protein−ligand binding.

Binding Isotherm for the Interaction of MonoUb with RAP80−tUIM. The dissociation constant for the RAP80-tUIM−monoUb interaction ($K_{D,mono}$) was determined experimentally as follows: $K_{D,mono}$ values for both the N- and C-terminal UIMs were extracted from a global fit of all [U-^{15}N, U-^{2}H]RAP80-tUIM residues with significant chemical shift changes upon addition of monoUb, and that could be followed unambiguously throughout the titration. Resonances from residues belonging to either UIM can be monitored separately by 2D $^1H-^{15}N$ HSQC NMR spectra, allowing for determination of individual $K_{D,mono}$ values for both UIMs. This was accomplished by simultaneously fitting all resonances from the N-terminal UIM with significant chemical shift changes to one $K_{D,mono}$ value, and the C-terminal resonances to a different $K_{D,mono}$. The equation representing the fractional chemical shift changes for a given UIM in RAP80 was modified to account for the binding of Ub to the other UIM, allowing for simultaneous monitoring of binding to both UIMs.

Thermodynamic Models for the Interaction between RAP80-tUIM and PolyUb Chains. In order to analyze NMR-based titrations of polyUb chains with RAP80-tUIM, we designed models to take into account both the basic multivalent interaction between tandem UIM units and tandem diUb units, and realistic interactions between individual UIM and individual Ub moieties within chains,

(9) Swanson, K. A.; Kang, R. S.; Stamenova, S. D.; Hicke, L.; Radhakrishnan, I. *EMBO J.* **2003**, *22*, 4597–4606.
(10) Sims, J. J.; Cohen, R. E. *Mol. Cell* **2009**, *33*, 775–783.
(11) Sato, Y.; Yoshikawa, A.; Mimura, H.; Yamashita, M.; Yamagata, A.; Fukai, S. *EMBO J.* **2009**, *28*, 2461–2468.
(12) Marley, J.; Lu, M.; Bracken, C. *J. Biomol. NMR* **2001**, *20*, 71–75.
(13) Sattler, M.; Schleucher, J.; Griesinger, C. *Prog. Nucl. Magn. Reson. Spectrosc.* **1999**, *34*, 93–158.

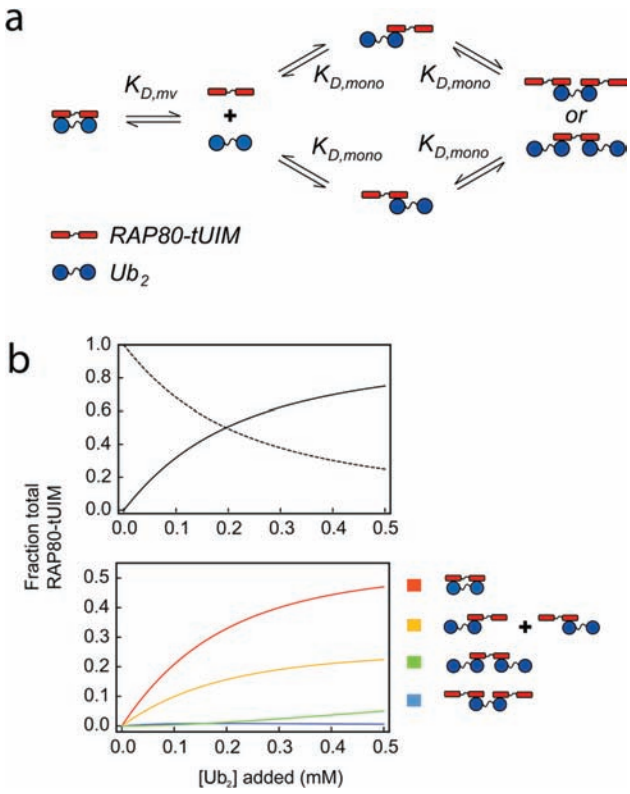

Figure 1. (a) Equilibria for the interaction between RAP80-tUIM and Ub_2. $K_{D,mv}$ (223 μM) denotes the dissociation constant for the multivalent interaction between both UIMs and both Ub moieties of Ub_2, whereas $K_{D,mono}$ (936 μM) is the dissociation constant for the interaction between a single UIM of RAP80 and a single Ub from Ub_2. (b) Simulated curves illustrating the buildup of various UIM−Ub_2 species as Ub_2 is added to 0.1 mM RAP80-tUIM. Curves show the fraction of total UIM in a particular state as a function of [Ub_2]. For the upper plot, the solid curve shows the sum of all RAP80-tUIM−Ub_2 states and the dashed curve shows the fraction of free RAP80-tUIM.

as well as states resulting from mixtures of both (Supporting Information). Equilibria for bound states are expressed in terms of a multivalent $K_{D,mv}$ (the interaction between RAP80-tUIM and two adjacent Ub molecules) and/or the $K_{D,mono}$ for monoUb binding. Expressions for the various equilibria for monoUb, as well as tandem Ub_2, Ub_3, and Ub_4 binding to RAP80-tUIM, are given in the Supporting Information. The basic multivalent binding model involves the interaction between the two UIM domains from RAP80, and the two Ub moieties from Ub_2. A schematic diagram for this model, and associated binding curves, are shown in Figure 1.

$K_{D,mv}$ values for RAP80-tUIM binding to Ub_2, Ub_3, and Ub_4 were determined by globally fitting backbone ^{15}N and ^{1}H chemical shift changes for all residues of RAP80-tUIM that could be followed unambiguously throughout the 2D ^{1}H−^{15}N HSQC or TROSY HSQC titrations by use of an in-house simulated annealing algorithm. The bound fraction is related to the NMR chemical shift changes through $\Delta\delta_{obs} = f_b\Delta\delta_{sat}$, where f_b is the theoretical bound fraction of [U-^{2}H, U-^{15}N]- or [U-^{15}N]-labeled protein (RAP80-tUIM or polyUb) at given RAP80-tUIM and polyUb concentrations, $\Delta\delta_{sat}$ is the maximum chemical shift change (corresponding to the saturated state), and $\Delta\delta_{obs}$ is the chemical shift change at given values for $K_{D,mv}$ and RAP80-tUIM and polyUb concentrations. $K_{D,mv}$ was optimized as follows: Theoretical $\Delta\delta_{obs}$ values for [U-^{2}H, U-^{15}N]- or [U-^{15}N]-labeled protein (RAP80-tUIM or polyUb) at concentrations used in the titrations were generated by initially setting the value of $K_{D,mv}$, and subsequently numerically solving the coupled equilibrium expressions given in the Supporting Information. The procedure was repeated by parametrically varying the value of $K_{D,mv}$ with a simulated annealing algorithm to minimize the sum of the squared differences between the experimental and theoretical chemical shift changes.

In addition to $K_{D,mv}$, the bound chemical shifts were treated as adjustable parameters during the fits, given that the combination of low-affinity binding and finite protein concentrations made saturation difficult to achieve. In the case of the [U-^{2}H, U-^{15}N]- or [U-^{15}N]-labeled RAP80-tUIM titrations with polyUb, starting values and constraints for these parameters could be selected on the basis of the final point (highest concentration of polyUb), given that they appear close to saturation. However, for the corollary titrations of the various [U-^{2}H, U-^{15}N]- or [U-^{15}N]-labeled polyUb chains, starting values and constraints were obtained from the final point of [U-^{15}N]Ub_2 titrated with RAP80-tUIM, the titration closest to saturation (72:1 UIM/Ub_2), which consequently likely represents the most accurate estimates of the bound Ub_2 chemical shifts. This approach has the implicit assumption that the bound chemical shifts of the various polyUb chains are the same upon saturation with RAP80-tUIM. This is reasonable, given that the direction and magnitude of chemical shift changes observed during the titrations are similar.

Errors in the optimized parameters were estimated by Monte Carlo trials of the global fits, based on the error in protein concentrations, determined by the bicinchoninic acid (BCA) assay, estimated to be 10%. The accuracy of the BCA assay with respect to determining RAP80-tUIM concentration was confirmed by amino acid analysis, the difference in concentration between the two measurement techniques being less than 2%.

Line-Shape Analysis for RAP80-tUIM Interaction with Ub_2. An analytical expression for the frequency domain NMR spectrum in the presence of two-site exchange was derived from the Bloch−McConnell equations,[14] modified to account for the application of a cosine-squared window function. NMR spectra were corrected for concentration differences and number of acquired transients and were numerically fit to the expression for the frequency domain spectrum by optimizing the values of k_{off}, the bound chemical shift, and a global intensity parameter.

Temperature Dependence of $^{13}C_\alpha$ and $^{1}H_\alpha$ Chemical Shifts of RAP80-tUIM. The temperature dependence of the main-chain $^{13}C_\alpha$ and $^{1}H_\alpha$ chemical shifts from 5 to 50 °C were used to characterize the helix−coil transition for RAP80-tUIM.[15] Briefly, the observed chemical shift changes as a function of temperature were fit to a two-state cooperative helix−coil transition (eq 9 in ref 16) using as fitted parameters the $^{13}C_\alpha$ or $^{1}H_\alpha$ chemical shifts for the α-helical and random coil states, as well as the midpoint and width of transition.

Main-Chain ^{15}N Relaxation Measurements for RAP80-tUIM. ^{15}N-R_1, R_2, and {^{1}H}−^{15}N nuclear Overhauser effect (NOE) relaxation data were acquired at 5 and 25 °C and two field strengths (600 and 800 MHz) as previously described.[17] Additionally, changes in ^{15}N-R_2 (600 MHz and 25 °C) for free RAP80-tUIM upon binding Ub_2 were also determined.

Contributions from chemical exchange (R_{ex}) to ^{15}N-R_2 were estimated by use of ^{15}N-R_1, R_2, and {^{1}H}−^{15}N NOE relaxation data combined with η_{xy} and η_z cross-correlated relaxation rates.[18] Additionally, a series of main-chain amide ^{1}H−^{15}N single and multiple quantum coherence and two-spin order relaxation rates

(14) Palmer, A. G.; Kroenke, C. D.; Loria, J. P. *Methods Enzymol.* **2001**, *339*, 204–238.
(15) Shalongo, W.; Dugad, L.; Stellwagen, E. *J. Am. Chem. Soc.* **1994**, *116*, 2500–2507.
(16) Nesmelova, I.; Krushelnitsky, A.; Idiyatullin, D.; Blanco, F.; Ramirez-Alvarado, M.; Daragan, V. A.; Serrano, L.; Mayo, K. H. *Biochemistry* **2001**, *40*, 2844–2853.
(17) Farrow, N. A.; Muhandiram, R.; Singer, A. U.; Pascal, S. M.; Kay, C. M.; Gish, G.; Shoelson, S. E.; Pawson, T.; Forman-Kay, J. D.; Kay, L. E. *Biochemistry* **1994**, *33*, 5984–6003.
(18) Kroenke, C. D.; Loria, J. P.; Lee, L. K.; Rance, M.; Palmer, A. G. *J. Am. Chem. Soc.* **1998**, *120*, 7905–7915.

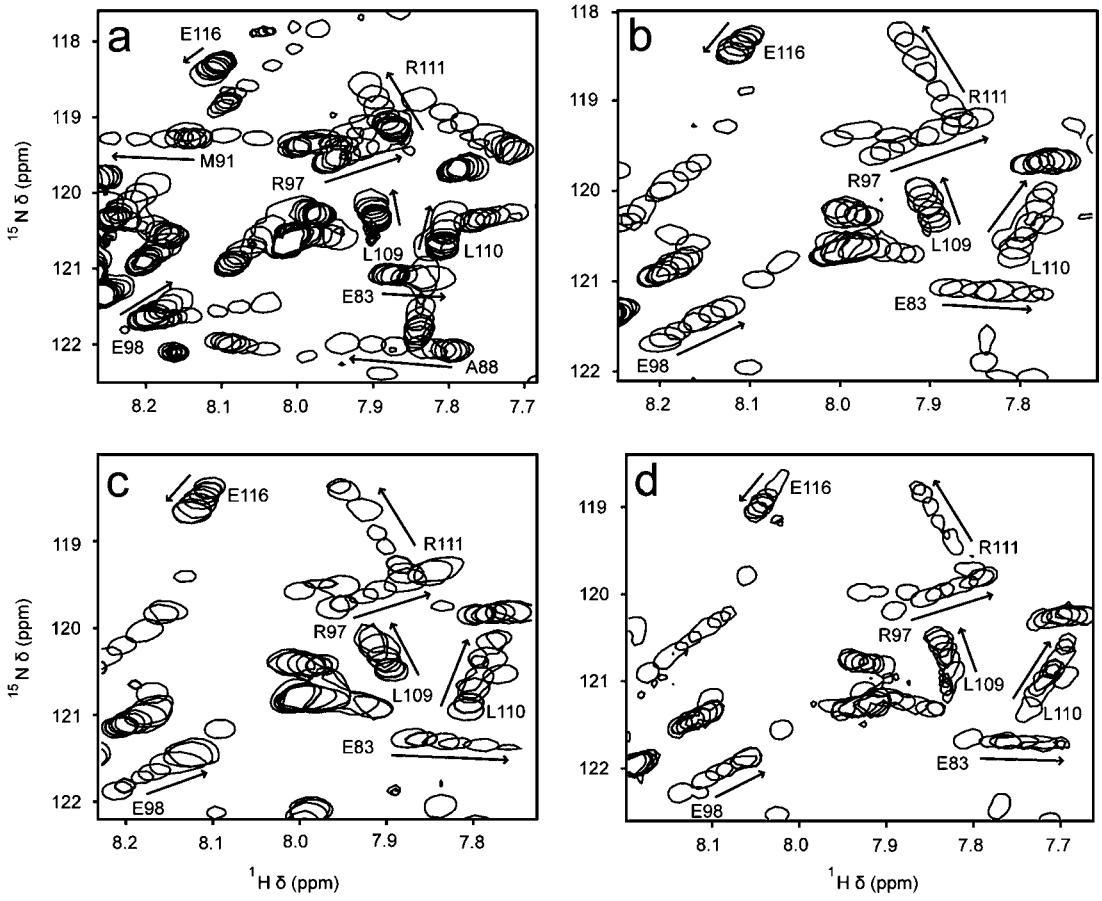

Figure 2. Representative regions from 2D ^{1}H−^{15}N HSQC NMR spectra of [U-^{15}N, U-^{2}H]RAP80-tUIM or [U-^{15}N]RAP80-tUIM titrated with (a) unlabeled Ub, (b) Ub_2, (c) Ub_3, and (d) Ub_4. Arrows indicate the direction of chemical shift changes upon polyUb addition for labeled RAP80-tUIM resonances.

were used to estimate the rate of chemical exchange for the main-chain amides.[19,20]

Molecular Dynamics Simulation and iRED Analysis for RAP80-tUIM. Calculations were conducted with the AMBER 10 simulation package,[21] with the ff99SB force field and the TIP3P water model. Covalent bonds to hydrogen were restrained by use of SHAKE, temperature was regulated by Langevin dynamics with a collision frequency of 1 ps^{-1}, and the cutoff was 8 Å for pairwise nonbonded and electrostatic interactions. A PME approach with default parameters was used for calculating long-range electrostatics. The initial structural model was solvated in a truncated octahedral water box with a minimum of 24 Å between a given protein atom and a given atom of an image in an adjacent unit cell. Six Na^+ ions were included to ensure the system was neutral. The system was heated gradually over 50 ps to 298 K with 2 kcal/mol restraints on solute atoms and equilibrated to 1 atm pressure for an additional 50 ps. Production dynamics were then conducted for 8 ns. The isotropic reorientational eigenmode (iRED) approach was used to extract correlation functions for the main chain amide $^{15}N-^{1}H^{N}$ vectors from the molecular dynamics simulation.[22] The correlation functions were fit to two-parameter monoexponential decays to extract correlation times; these were subsequently used to calculate ^{15}N-R_1, R_2, and NOE values at 600 and 800 MHz.

Molecular Dynamics Simulation for Tandem Ub_3. Molecular dynamics were carried out with the AMBER 10 biomolecular simulation software suite. The ff99SB force field was employed with the "GBn" generalized Born solvation model with a salt concentration of 150 mM, covalent bonds to hydrogen were restrained by use of SHAKE, and there were no cutoffs for nonbonded interactions and a 25 Å cutoff for pairwise summation of effective Born radii. Temperature was regulated by Langevin dynamics with a collision frequency of 50 ps^{-1}. The system was heated from 0 to 300 K over 50 ps with a time step of 2 fs. Production dynamics were run for 80.5 ns. Cross-correlation functions for vectors from the first two Ub moieties in Ub_3, either perpendicular or parallel to the long axis of the extended Ub_3 chain, were calculated and fit to monoexponential decays to determine the correlation times for reorientation of Ub moieties with respect to each other.

Results and Discussion

Interaction of RAP80-tUIM with Ub, Tandem Ub_2, Tandem Ub_3, and Tandem Ub_4. The interaction between RAP80-tUIM and various tandem polyUb chains was analyzed via NMR-based titrations for both binding partners. We titrated [U-^{15}N]- or [U-^{15}N, U-^{2}H]RAP80-tUIM with unlabeled Ub, Ub_2, Ub_3, and Ub_4 chains (Figure 2) and carried out corollary titrations of [U-^{15}N]Ub_2, [U-^{15}N]Ub_3, and [U-^{15}N, U-^{2}H]Ub_4 with unlabeled RAP80-tUIM to ensure consistency. The maximum chemical shift changes observed in these titrations are shown in Figure 3. For RAP80-tUIM, these changes occur within the α-helical UIM domains and predominantly at the canonical I44 hydrophobic binding site for polyUb.

The NMR-derived binding curves were initially analyzed with the assumption of 1:1 binding to extract macroscopic dissocia-

(19) Hansen, D. F.; Yang, D.; Feng, H.; Zhou, Z.; Wiesner, S.; Bai, Y.; Kay, L. E. *J. Am. Chem. Soc.* **2007**, *129*, 11468–11479.
(20) Hansen, D. F.; Feng, H.; Zhou, Z.; Bai, Y.; Kay, L. E. *J. Am. Chem. Soc.* **2009**, *131*, 16257–16265.
(21) Case, D. A. AMBER10; University of California, San Francisco, 2008.
(22) Prompers, J. J.; Brüschweiler, R. *J. Am. Chem. Soc.* **2002**, *124*, 4522–4534.

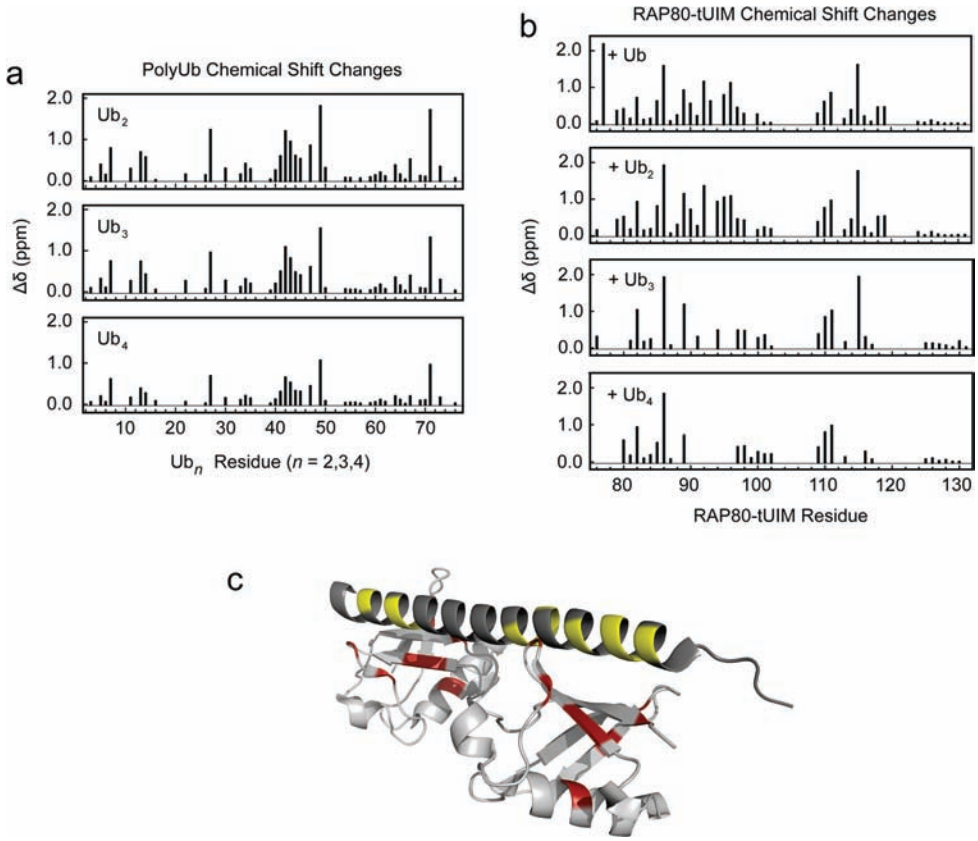

Figure 3. Maximum polyUb chemical shift changes, $\Delta\delta = [(\Delta\delta\ ^{15}N)^2 + (\Delta\delta\ ^{1}H^N)^2]^{1/2}$, observed in titrations of [U-^{15}N, U-^{2}H]- or [U-^{15}N]-labeled polyUb chains with unlabeled RAP80-tUIM (a), and RAP80-tUIM $\Delta\delta$ upon titration of [U-^{15}N, U-^{2}H]- or [U-^{15}N]-labeled RAP80-tUIM with unlabeled polyUb chains (b). Residues 103−108 are a stretch of contiguous Glu residues that are unassigned. Shown in panel c are chemical shift changes exceeding the median by 1 standard deviation ($\langle\Delta\delta\rangle + 1\sigma$) for the RAP80-tUIM−$Ub_2$ titrations, mapped on the RAP80-tUIM−Ub_2 structure, with $\langle\Delta\delta\rangle + 1\sigma$ values for RAP80 in yellow and those for Ub_2 in red. $\Delta\delta$ values for several RAP80-tUIM residues were not observed upon titration with Ub_3 and Ub_4 due to line broadening as a result of increased molecular weight of the complexes and chemical exchange. PolyUb and RAP80-tUIM $\Delta\delta$ values are observed to shift in a similar manner in the titrations. Differences in the overall magnitude of $\Delta\delta$ for titrations of longer polyUb chains with unlabeled RAP80-tUIM (a) are likely due to lower levels of saturation resulting from an increased number of binding sites on the longer chains (Supporting Information).

tion constants, followed by more detailed analyses wherein we assumed that the RAP80-tUIM interaction with polyUb involves two equilibrium constants: $K_{D,mono}$, the dissociation constant for the interaction between a given UIM from RAP80 and monoUb, and $K_{D,mv}$, the multivalent dissociation constant for the simultaneous interaction between both RAP80 tandem UIMs and two neighboring intramolecular Ub moieties within a polyUb chain (Figure 1a). These detailed analyses of the titrations indicate that the increased macroscopic 1:1 binding affinity observed as a function of increasing chain length can be explained by an increased number of multivalent binding sites in the longer polyUb chains, as well as an increased number of low-affinity interactions between single UIMs from RAP80 with individual Ub moieties in the chain.

Simple Analyses of RAP80-tUIM−PolyUb Binding. NMR-based titrations of unlabeled monoUb into [U-^{15}N, U-^{2}H]RAP80-tUIM indicate that the tandem RAP80 UIMs bind monoUb weakly, with similar dissociation constants ($K_{D,mono}$) for the N- and C-terminal UIMs (Figure 4 and Table 1). The similar $K_{D,mono}$ values for Ub binding to either the N- or C-terminal UIM are reflected in the lack of an initial lag phase in chemical shift titration curves for residues located in either helix.

We obtained an initial view of affinity changes with increasing polyUb chain length by analyzing the NMR-based titrations, assuming 1:1 binding. Using this first approach, the RAP80-tUIMs bind tandem Ub_2, Ub_3, and Ub_4 with increasing affinity upon increasing chain length, having macroscopic dissociation constants that decrease 12-, 55-, and 59-fold, respectively, in comparison to monoUb binding (Table 1). These macroscopic dissociation constants indicate similar multivalent effects for Lys63-linked[10] and tandem Ub chains, with a (24 ± 6)-fold increase in affinity for Lys63-linked polyUb chains compared to a (13 ± 5)-fold increase for tandem polyUb chains, for Ub_2 binding in comparison to monoUb binding. Increases in affinity with increasing chain length are the same for the two types of chains within error, with (5.5 ± 0.4)- and (5 ± 2)-fold increases for Ub_4 in comparison to Ub_2 binding, for Lys63-linked and tandem chains, respectively. These results suggest that binding interactions for tandem and K63-linked Ub chains are similar for RAP80-tUIM, as observed for polyUb binding to NEMO,[23] and that tandem polyUb chains serve as reasonable models to understand the molecular basis of polyUb chain recognition by tandem UIMs.

The RAP80-tUIM−Tandem Ub_2 Interaction Is Specific and Multivalent. The binding of RAP80-tUIM to Ub_2 encompasses the fundamental molecular basis, or unit, for recognition of polyUb chains by RAP80-tUIM (Figures 1 and 3c). The titration of [U-^{15}N]-tandem Ub_2 with unlabeled RAP80-tUIM indicates that the UIMs of RAP80 bind in a multivalent manner

(23) Lo, Y. C.; Lin, S. C.; Rospigliosi, C. C.; Conze, D. B.; Wu, C. J.; Ashwell, J. D.; Eliezer, D.; Wu, H. *Mol. Cell* **2009**, *33*, 602–615.

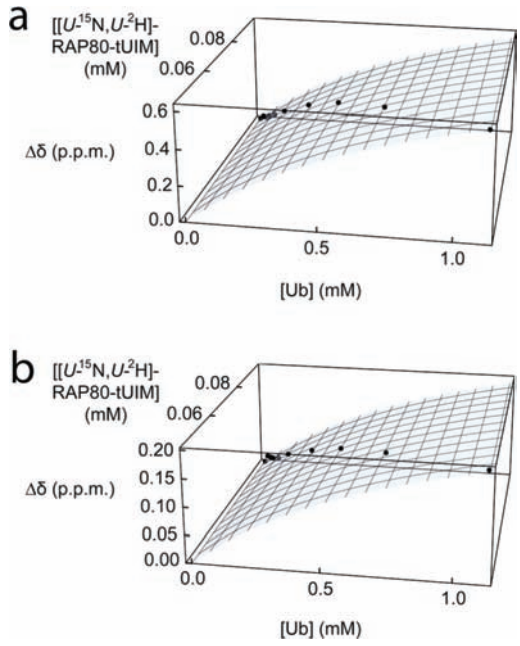

Figure 4. Titration of [U-^{15}N, U-^{2}H]RAP80-tUIM with unlabeled Ub. (a) ^{15}N chemical shift changes for F85 within the N-terminal UIM are indicated on the vertical axis, and concentrations of analyte or titrand (labeled RAP80-tUIM) and unlabeled Ub titrant are indicated on the horizontal axes. (b) ^{15}N chemical shift changes for E116, within the C-terminal UIM. Experimentally determined chemical shift changes are shown as points, and the best fits to associated binding isotherms are shown as surfaces (Materials and Methods and Supporting Information).

Table 1. Dissociation Constants for 1:1 Binding of RAP80-tUIM to Ub, Tandem Ub Chains, and K63-Linked Ub Chains

K_D (μM)[a]						
Ub	tUb_2[b]	K63-Ub_2[c]	tUb_3	K63-Ub_3	tUb_4	K63-Ub_4
936 ± 240[d] 520 ± 130[e]	75 ± 26	22 ± 1[e]	17 ± 7	nd[f]	16 ± 7	4.0 ± 0.2[e]

[a] K_D values were determined with the assumption of 1:1 binding. [b] tUb_n indicates tandem Ub chains (n = 2, 3, 4) linked sequentially through respective N- and C-termini. [c] K63-Ub_n indicates Ub chains (n = 2, 3, 4) linked sequentially through respective K63 residues and C-termini. [d] Average $K_{D,mono}$ for UIM1 (930 ± 162 μM) and UIM2 (942 ± 177 μM), determined in this study by NMR. [e] Determined by fluorescence anisotropy (ref 10). [f] Not determined.

to Ub_2. That is, the individual RAP80 UIMs bind the individual Ub moieties in tandem Ub_2 in a specific orientation. For example, the ^{1}H−^{15}N HSQC NMR spectrum of Ub_2 alone closely resembles that of monoUb. However, as RAP80-tUIM is added, a number of the Ub_2 resonances that respond to UIM binding diverge into two peaks, both of which are in fast exchange with unbound Ub_2 (Figure 5). This is likely due to sequence differences between the N- and C-terminal UIM domains that give rise to different bound chemical shifts for labeled Ub_2. Importantly, this indicates that the individual Ub moieties of Ub_2 favor one of the tandem UIMs, which can occur only if nonpromiscuous, multivalent binding is present. These NMR results are consistent with the specific orientation observed for RAP80-tUIM bound to K63-linked Ub_2,[11] which indicates that multivalent binding occurs with the N-terminal Ub bound to the C-terminal UIM and the C-terminal Ub simultaneously bound to the N-terminal UIM. The observed peak splitting also demonstrates that tandem polyUb chains are reasonable mimics for K63-linked chains, with regard to their ability to facilitate

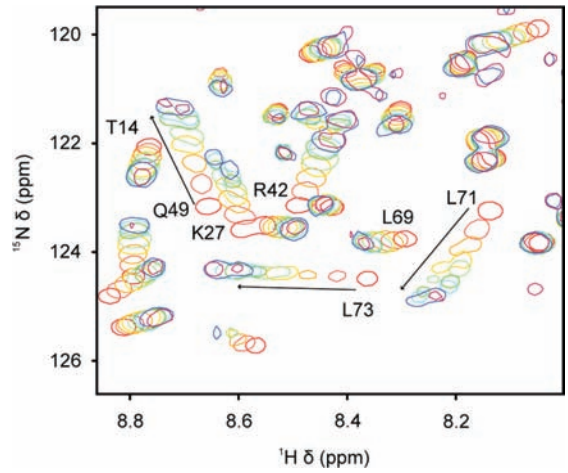

Figure 5. Region from the 2D ^{1}H−^{15}N HSQC NMR spectrum of [U-^{15}N]Ub_2 upon titration with unlabeled RAP80-tUIM. Splitting of monoUb resonances into two distinct peaks for various residues upon titration with unlabeled RAP80-tUIM are highlighted by black arrows.

multivalent binding of UIMs, a fact that is also borne out by the similar structures for K63-linked and tandem diUb.[24]

Multivalent Models for Analyses of Binding between RAP80-tUIM and PolyUb. The binding of RAP80-tUIM to polyUb chains was modeled by constructing equilibria for physically reasonable bound states for the various polyUb chains and assuming that the binding process is described by two dissociation constants: binding of a single Ub to a single UIM domain ($K_{D,mono}$) and multivalent binding of tandem UIMs to sequential diUb units within polyUb chains ($K_{D,mv}$) (Figure 1 and Supporting Information). These models assume that binding of both UIMs from a RAP80-tUIM molecule to sequential diUb units in a polyUb chain does not alter binding of either a single UIM from a RAP80-tUIM molecule to the adjacent free Ub sites or a second RAP80-tUIM unit to adjacent free sequential diUb units in polyUb chains. This assumption is reasonable given the flexibility between UIMs in RAP80-tUIM and between Ub moieties in tandem polyUb, which is discussed in detail in subsequent sections. Additionally, in order for binding of RAP80-tUIM to a sequential diUb unit in a polyUb chain to alter binding of other RAP80-tUIM molecules to immediately adjacent Ub moieties, one would expect a structural interaction between the long C-terminal tail of a bound RAP80-tUIM and the adjacent Ub moieties. However, no significant chemical shift changes for the C-terminal region of RAP80-tUIM are observed upon interaction with longer tandem Ub_3 and Ub_4 chains (Figure 3b).

$K_{D,mono}$ was experimentally determined, whereas $K_{D,mv}$ was determined by global fitting of NMR-based titrations of RAP80-tUIM with tandem Ub_2, Ub_3, and Ub_4. It should be noted that the common assumption that multivalent association constants are given by the product of individual constants is strictly not legitimate.[25,26] Indeed, affinity increases due to multivalent binding can be larger than expected, given an intrinsically low-affinity individual interaction.[27]

The values of $K_{D,mv}$ for multivalent polyUb binding, globally fit by use of NMR titrations of RAP80-tUIM with tandem Ub_2, Ub_3, and Ub_4 and the corollary titrations of RAP80-tUIM into

(24) Komander, D.; Reyes-Turcu, F.; Licchesi, J. D.; Odenwaelder, P.; Wilkinson, K. D.; Barford, D. *EMBO Rep.* **2009**, *10*, 466–473.
(25) Jencks, W. P. *Proc. Natl. Acad. Sci. U.S.A.* **1981**, *78*, 4046–4050.
(26) Zhou, H. X.; Gilson, M. K. *Chem. Rev.* **2009**, *109*, 4092–4107.
(27) Lee, R. T.; Lee, Y. C. *Glycoconjugate J.* **2000**, *17*, 543–551.

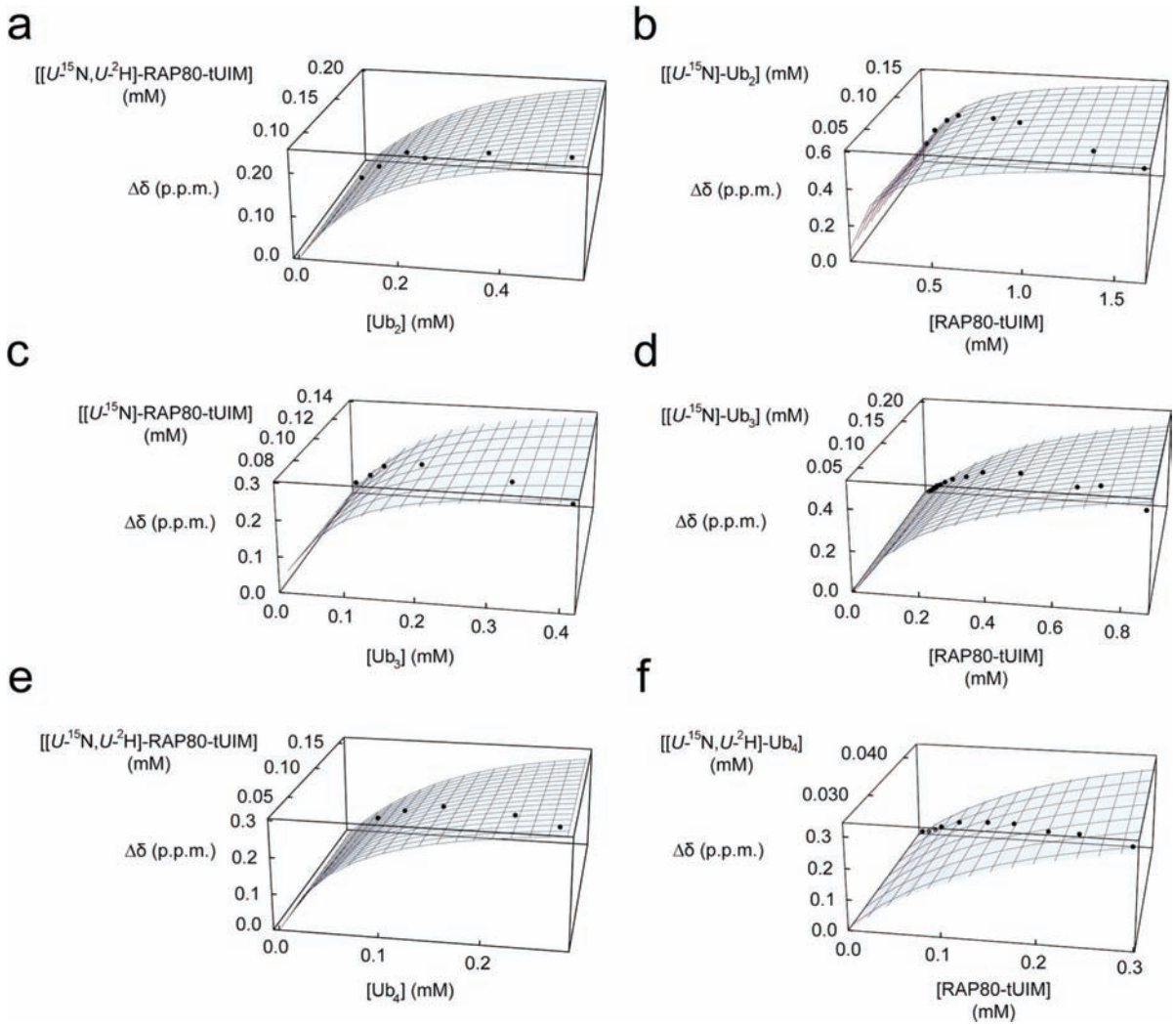

Figure 6. Fits of chemical shift perturbation data to multivalent binding models for RAP80-tUIM binding to polyUb. Experimental chemical shift changes are indicated on the vertical axis, and concentrations of analyte or titrand (labeled RAP80-tUIM in left panels, labeled polyUb in right panels) and unlabeled titrant (polyUb in left panels, RAP80-tUIM in right panels) are indicated on the horizontal axes. (a) ^{15}N chemical shift changes for E116 from [U-^{15}N, U-^{2}H]RAP80-tUIM titrated with unlabeled Ub_2. (b) ^{15}N chemical shift changes for I44 from [U-^{15}N]Ub_2 titrated with unlabeled RAP80-tUIM. (c) ^{15}N chemical shift changes for E116 from [U-^{15}N]RAP80-tUIM titrated with unlabeled Ub_3. (d) ^{15}N chemical shift changes for I44 from [U-^{15}N]Ub_3 titrated with unlabeled RAP80-tUIM. (e) ^{15}N chemical shift changes for E116 from [U-^{15}N, U-^{2}H]RAP80-tUIM titrated with unlabeled Ub_4. (f) ^{15}N chemical shift changes for I44 from [U-^{15}N, U-^{2}H]Ub_4 titrated with unlabeled RAP80-tUIM. Experimentally determined chemical shift changes are shown as points, and the best fits to associated binding isotherms are shown as surfaces (Materials and Methods and Supporting Information).

Table 2. Multivalent Dissociation Constants for Binding of RAP80-tUIM to Tandem Ub Chains

$K_{D,mv}$ (μM)[a]		
tUb_2[b]	tUb_3	tUb_4
150 ± 60[c]	80 ± 23[c]	200 ± 40[c]
200 ± 40[d]	400 ± 110[d]	320 ± 45[d]

[a] $K_{D,mv}$ values were determined from bound states and equilibria shown in Supporting Information. [b] tUb_n indicates tandem Ub chains (n = 2, 3, 4) linked sequentially through respective N- and C-termini. [c] Titration of tUb_n into [U-^{15}N]- or [U-^{15}N, U-^{2}H]RAP80-tUIM. [d] Titration of RAP80-tUIM into [U-^{15}N]- or [U-^{15}N, U-^{2}H]tUb_n.

tandem Ub_2, Ub_3, and Ub_4, are shown in Figure 6 and Table 2 and are in good agreement within experimental error. The average $K_{D,mv}$ of 223 ± 114 μM for the multivalent interaction is 4 times stronger than $K_{D,mono}$. The relatively weak $K_{D,mv}$ for the various polyUb titrations, compared to the increase in affinity with increasing chain length observed for analyses that assume 1:1 binding, underscores the advantage of employing multivalent binding for achieving a large increase in affinity from a fundamentally low-affinity interaction in a biological system. Our detailed analyses of the NMR-based titrations have allowed us to separate $K_{D,mv}$ from the macroscopic K_Ds that were determined with the assumption of 1:1 binding and which represent the sum over all binding modes (Table 1). The 4-fold difference between $K_{D,mono}$ and $K_{D,mv}$, combined with increased numbers of binding sites in longer polyUb chains, results in a 59-fold increase in the macroscopic affinity of RAP80-tUIM for tandem Ub_4 compared to monoUb.

The simplest molecular unit for multivalent binding of RAP80-tUIM to polyUb is characterized by the binding of RAP80-tUIM to Ub_2 (Figure 3c). From a molecular perspective, the multivalent dissociation constant can be understood as stepwise binding of one UIM, followed by binding of the second UIM, where the second binding event is considered to be intramolecular.[25] For this type of molecular model, the multivalent dissociation constant is given by

$$K_{D,mv} = K_{D,mono1}K_{D,mono2}/\rho_L(\mathbf{r}_0) \quad (1)$$

where $K_{D,mono1}$ is the dissociation constant for binding of the first UIM, $K_{D,mono2}$ corresponds to binding of the second UIM, and $\rho_L(\mathbf{r}_0)$ is the effective concentration, or probability density for the end-to-end length of the linker vector $\mathbf{r}_0$.[25] The effective concentration has typical values in the millimolar range for peptide linkers that are flexible.[25] Substituting the values of $K_{D,mono}$ and $K_{D,mv}$ for the RAP80-tUIM−polyUb interaction (Tables 1 and 2) into eq 1 and solving for $\rho_L(\mathbf{r}_0)$ gives an effective concentration of ∼4 mM. For K63-linked chains, the assumption that $K_{D,mv}$ is 22 μM (Table 1) gives $\rho_L(\mathbf{r}_0)$ ∼12 mM. The larger $\rho_L(\mathbf{r}_0)$ value for K63-linked chains is consistent with the greater affinity of RAP80-tUIM for K63-linked Ub_2. However, this straightforward analysis cannot separate differences in structural and entropic contributions to binding between tandem Ub_2 and K63-linked Ub_2 that are unrelated to linker length; binding differences are simply grouped together as changes in $\rho_L(\mathbf{r}_0)$. Furthermore, eq 1 assumes that the Ub_2 "receptor" is a rigid entity, whereas for both tandem and K63-Ub_2, the Ub moieties are linked by dynamic tethers and are flexible with respect to each other. The consequence of this effect in using eq 1 is that it will lead to lower-than-expected effective concentrations. Additionally, the assumption that $K_{D,mv}$ ∼ 22 μM for the RAP80-tUIM−Ub_2 interaction should be taken as a lower limit for $K_{D,mv}$, as the actual multivalent dissociation constant is most likely larger, given that this value was determined with the assumption of 1:1 binding, whereas the underlying interactions have more binding modes, which typically leads to a weaker $K_{D,mv}$ (Figure 1).

The effective concentration values for the interaction of RAP80-tUIM with tandem and K63-Ub_2 can be compared to multivalent binding of the tandem UIMs from S5a (S5a-tUIM), a ubiquitin receptor from the proteasome, to K48-linked Ub_2.[28] Given values of $K_{D,mono1}$ and $K_{D,mono2}$ of 350 and 73 μM, respectively, and if it is assumed that $K_{D,mv}$ is similar to the dissociation constant for the K48-Ub_2−S5a-tUIM interaction (9 μM), then $\rho_L(\mathbf{r}_0)$ ∼3 mM. The decrease in $\rho_L(\mathbf{r}_0)$ for the K48-Ub_2−S5a-tUIM interaction compared to the RAP80-tUIM interaction with tandem or K63-linked Ub_2 is consistent with the significantly longer inter-UIM linker (∼60 residues) compared to that of RAP80-tUIM (∼10 residues). However, the linker between UIMs in S5a has substantial stretches of α-helical structure (∼30 residues), whereas eq 1 is formulated under the assumption that the linker region is entirely flexible.

In addition to stepwise binding and effective concentration as a mechanism for multivalent binding in RAP80-tUIM, it is also possible that cooperative effects play a role. For example, binding of the first UIM may induce helical structure in the linker region, thereby stabilizing helical structure in the second UIM. Furthermore, conformational selection can also have an impact on the basic tandem UIM−Ub_2 interaction; these effects are discussed in more detail below.

We complemented our NMR-based equilibrium binding studies with measurements of the kinetics of binding and the dynamics of the individual interacting partners. These results indicate that gains in affinity from multivalent binding are balanced by dynamic effects to provide a combined driving force for recognition of extended polyUb chains; this balance between enthalpy and entropy may have physiological relevance with respect to initiating transient protein−protein complexes at sites of DNA damage.

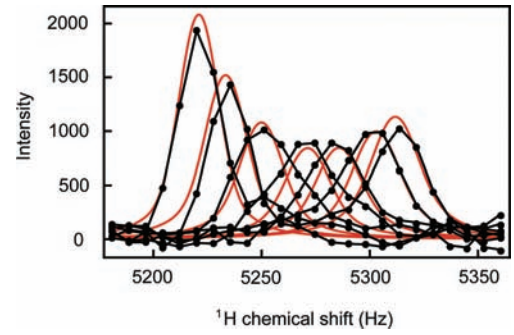

Figure 7. Line-shape analysis for [U-^{15}N]RAP80-tUIM E81 $^1H^N$ upon titration with tandem Ub_2. Experimental data are shown in black, and the fit is shown in red.

Binding Kinetics for the RAP80-tUIM−Ub_2 Interaction. The kinetics of the interaction between RAP80-tUIM and tandem Ub_2 were determined with the assumption of 1:1 binding and by use of line-shape analysis for ^{1}H−^{15}N HSQC NMR spectra acquired during the titration of unlabeled Ub_2 into [U-^{15}N, U-^{2}H]RAP80-tUIM, to yield estimates of ∼1.4 × 10^8 M^{-1} s^{-1} and ∼10 000 s^{-1} for k_{on} and k_{off}, respectively (Figure 7). This fast off-rate has important implications for signal amplification through multivalent binding utilizing numerous weak interactions. The likely role of the polyUb signal in the DNA damage response is to act as a transient initiator of dynamic protein−protein complexes at sites of damage. From a physiological standpoint, multivalent binding that is inherently weak with fast kinetics ensures that temporal and spatial fluctuations of protein−protein signaling cascades, such as those initiated by recognition of polyUb chains, occur on rapid time scales.

Conformational Selection and UIM−Ub Recognition: Impact of the UIM Helix−Coil Transition. The helix−coil transition for the RAP80-tUIM α-helices may have a significant impact on the binding of Ub and polyUb chains. The transition for RAP80-tUIM was studied by following the temperature dependence of main-chain $^1H_\alpha$ and $^{13}C_\alpha$ chemical shifts (Figure 8) and was assumed to obey a two-state, cooperative unfolding process, yielding a melting temperature of 34 °C, a thermal transition width of 28 °C, and per-residue chemical shift differences between helical and unfolded states. The width of the thermal transition is defined as the temperature range that covers the middle 80% of the transition (eq 1 in ref 15). Thus, at 25 °C, the α-helices of RAP80-tUIM are ∼70% helical. These results are consistent with similar studies using α-helical peptides.[16] The kinetics of the helix−coil transition was characterized by measuring cross-correlated main-chain amide ^{1}H−^{15}N single quantum coherence and two-spin order relaxation rates,[18] and a series of main-chain amide ^{1}H−^{15}N single and multiple quantum coherence and two-spin order relaxation rates.[19,20] The resulting average rate of chemical exchange (R_{ex}) for the α-helices at 5 °C, presumably arising from the helix−coil transition, is 1.0 ± 0.8 s^{-1}. This R_{ex} value can be used to determine an approximate estimate for the rate of exchange (k_{ex}) for the helix−coil transition[19]

$$R_{ex} \approx \frac{p_H p_C \Delta\omega^2 k_{ex}}{\Omega_C^2 + \omega_1^2 + k_{ex}^2} \quad (2)$$

(28) Zhang, N.; Wang, Q.; Ehlinger, A.; Randles, L.; Lary, J. W.; Kang, Y.; Haririnia, A.; Storaska, A. J.; Cole, J. L.; Fushman, D.; Walters, K. J. *Mol. Cell* **2009**, *35*, 280–290.

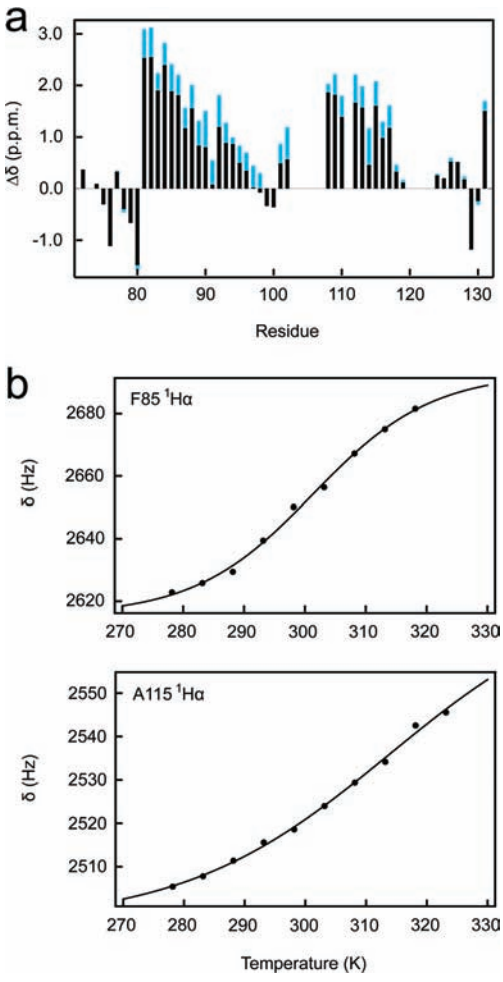

Figure 8. (a) Deviation from random coil $^{13}C_\alpha$ chemical shifts for [U-^{13}C, U-^{15}N]RAP80-tUIM, at 5 °C (blue) and 25 °C (dark gray). Residues 104−107 are a stretch of contiguous Glu residues that are unassigned. (b) Temperature dependence of $^{1}H_\alpha$ chemical shifts for F85 and A115 from [U-^{13}C, U-^{15}N]RAP80-tUIM.

where ω_1 is the spin-lock field strength (radians per second); $\Delta\omega = \Omega_H - \Omega_C$ (radians per second), where Ω_H and Ω_C are the offset frequencies for the helix and coil states from the carrier frequency (radians per second), respectively; $k_{ex} = k_f + k_u$, where k_f and k_u are the folding and unfolding rate constants (per second), respectively; and p_H and p_C are the fractional populations of the helix and coil states. For $p_H = 0.9$ at 5 °C, determined from the temperature dependence of $^{13}C_\alpha$ and $^{1}H_\alpha$ chemical shifts, an assumed ^{15}N chemical shift difference between states of 5 ppm, and an ^{15}N spin-lock field strength of 1.8 kHz, we calculate an R_{ex} value of $\sim 1\ s^{-1}$, using a value for k_{ex} of $\sim 3 \times 10^5\ s^{-1}$, or $\tau_{ex} \sim 1/k_{ex} \sim 3\ \mu s$. This estimate for the rate of exchange due to the helix−coil transition is consistent with previous NMR[16] and temperature jump[29] measurements, which indicate that τ_{ex} for the helix−coil transition is 0.1−1 μs.

The helix−coil transition for the α-helices within RAP80-tUIM has the potential to alter the meaning of the macroscopic binding affinity. Assuming that Ub binds only the α-helical state of the UIM, that is, binding is governed by conformational selection,[30] we estimate that the macroscopic dissociation constants determined by NMR may be too large by about 4-fold for the basic multivalent RAP80-tUIM−Ub_2 interaction. For example, consider the following expression for the concentration of bound protein in a 1:1 protein−ligand interaction:

$$[PL] = \{K_{D1} + L_0 + P_0 + [K_{D1}^2 + (L_0 - P_0)^2 + 2K_{D1}(L_0 + P_0)]^{1/2}\}/2 \quad (3)$$

where L_0 is the total concentration of ligand, given by the sum of free ligand [L] and ligand bound to protein ([PL]), P_0 is the total protein concentration, given by the sum of free protein [P] and protein bound to ligand ([PL]), and K_{D1} is the dissociation constant for the protein−ligand interaction. Including an equilibrium between α-helical and unfolded states for the ligand in a 1:1 protein−ligand interaction, and assuming that the protein only binds ligand that is in the α-helical conformation (conformational selection), gives the following expression:

$$[PL_H] = \{K_{D2} + K_{D2}K_H + K_H L_0 + K_H P_0 - [4K_{D2}K_H(1 + K_H)L_0 + (K_{D2} + K_{D2}K_H - K_H L_0 + K_H P_0)^2]^{1/2}\}/2K_H \quad (4)$$

P_0 is the total protein concentration, given by the sum of free protein [P] and protein bound to ligand in the α-helical state ([PL_H]); L_0 is the total concentration of ligand, given by the sum of free ligand in the coil state [L_C], ligand in the α-helical state [L_H], and ligand in the α-helical state bound to protein ([PL_H]). K_{D2} is the dissocation constant for the interaction between protein and α-helical ligand, and $K_H = 1/p_H$, where p_H is the fraction of ligand in the α-helical conformation. For $p_H = 0.7$ (the fraction of a given RAP80 UIM in the α-helical conformation at 25 °C), $K_{D1} = 900\ \mu$M (similar to $K_{D,mono}$), $P_0 = 1$ mM, and $L_0 = 2$ mM, eqs 3 and 4 predict that, for $K_{D1} = K_{D2}$, conformational selection causes the macroscopic binding isotherm to appear as though binding is weaker, that is, [PL]/[PL_H] = 1.2 for $P_0 = 1$ mM, and $L_0 = 2$ mM. If K_{D2} is decreased by a factor of 1.6, giving an apparent increase in affinity, then the binding isotherms have a similar appearance with [PL]/[PL_H] = 1.

The impact of conformational selection in the multivalent binding models can be assessed in the simplest sense by inspection of eq 1. If both the UIM domains from RAP80 are in equilibrium between the α-helical and unfolded states, and polyUb binds only the α-helical conformation, both $K_{D,mono1}$ and $K_{D,mono2}$ are underestimated by a factor of 2. Therefore, exclusion of conformational selection in the multivalent binding models gives a 4-fold overestimate of $K_{D,mv}$; that is, the apparent affinity of the basic multivalent interaction is reduced by conformational selection.

Thus, gains in affinity through multivalent binding are at least partly offset by conformational selection effects arising from the helix−coil transition for the UIM. Balancing affinity gains due to multivalent binding may be important in maintaining transient, dynamic protein−protein complexes at sites of DNA damage undergoing repair processes. Finally, we cannot rule out that an induced-fit mechanism plays a role in the basic, multivalent RAP80-tUIM−Ub_2 interaction. Specifically, binding of one UIM from RAP80 may induce the cooperative formation of α-helical structure in the second UIM α-helix through the linker. Indeed, it has been shown for 1:1 enzyme−ligand binding, wherein the enzyme is in equilbrium between tight and weak ligand binding forms and the rate constants for the underlying equilibria are known, that the flux through both

(29) Eaton, W. A.; Munoz, V.; Thompson, P. A.; Henry, E. R.; Hofrichter, J. *Acc. Chem. Res.* **1998**, *31*, 745–753.
(30) Kumar, S.; Ma, B.; Tsai, C. J.; Sinha, N.; Nussinov, R. *Protein Sci.* **2000**, *9*, 10–19.

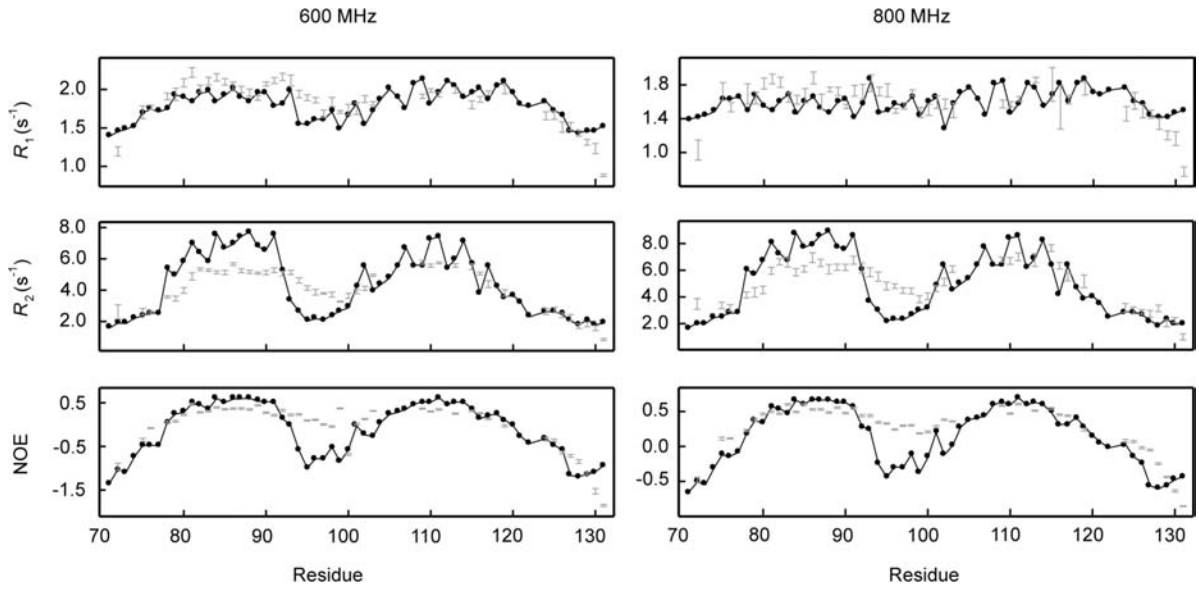

Figure 9. Main-chain amide ^{15}N-R_1, R_2, and NOE data at 25 °C, and 600 and 800 MHz for [U-^{15}N]RAP80-tUIM. Experimental data are shown as gray bars, and relaxation parameters calculated via iRED analysis are shown as black circles.

mechanisms can vary, one mechanism can be favored, or they can occur simultaneously, depending on the enzyme and ligand concentration ratios.[31]

Main-Chain Dynamics of RAP80-tUIM: Impact on Multivalent PolyUb Binding and Conformational Selection. Fast, pico- to nanosecond time scale fluctations, or tier-1 and tier-2 dynamics,[32] for the protein main chain are often characterized by ^{15}N-R_1, R_2, and NOE NMR relaxation measurements.[33−35] These motions play key roles in molecular processes that determine the affinities of proteins for ligands and other proteins, protein stability, and the catalytic activity of enzymes.[32] Pico- to nanosecond time scale fluctutations determined by NMR relaxation methods are frequently simulated by molecular dynamics and have the potential to provide important insights into the fundamental determinants of molecular motions.[22,36] In this study, the isotropic reorientational eigenmode (iRED) molecular dynamics approach[22] was used to simulate ^{15}N-R_1, R_2, and NOE NMR relaxation parameters for the main chain of RAP80-tUIM at 25 °C. The iRED approach has allowed us to investigate the role of tier-1 and tier-2 dynamics in the structure and stability of the UIM domains from RAP80 and the role that flexibility between these domains plays with respect to multivalent binding.

The experimental relaxation data at 25 °C and magnetic field strengths of 600 and 800 MHz are in good agreement with those calculated from the molecular dynamics simulation using the iRED general framework (Figure 9 and Figure S1 in Supporting Information). However, it should be noted that rapid exchange ($k_{ex} > 3 \times 10^5$ s^{-1}) of the α-helical regions between the helical and unfolded states can be expected to give rise to experimental ^{15}N-R_1, R_2, and NOE values that are a weighted average between these states. In addition, the R_2 values may have small contributions (<1 s^{-1} at 5 °C) arising from chemical exchange due to the helix−coil transition. Thus, experimental R_1 values can be expected to be smaller than those for a rigid helix, experimental R_2 values larger than expected (in the absence of chemical exchange contributions), and NOE values smaller than expected. Additionally, various AMBER force fields are known to overestimate the rigidity of isolated α-helices; indeed, the N- and C-terminal α-helices are ∼95% helical over the time course of the molecular dynamics simulation, as calculated by the DSSP algorithm. Consistent with this and the expected averaging of the relaxation rates due to fast exchange between helical and unfolded conformations, the experimental NOE values are smaller in magnitude than the simulated values, with rmsd values of 0.3 and 0.2 at 600 and 800 MHz. The simulated R_2 values have rmsd values at both fields of ∼1 s^{-1} and appear to be overestimated at 600 but not at 800 MHz. The R_1 values are generally in good agreement between experiment and the simulation, with rmsd values of ∼0.2 s^{-1} at 600 and 800 MHz. With respect to expected R_1 decreases due to rapid averaging, we note that, for a relatively rigid protein, the R_1 value is less sensitive to motions with correlation times in the 1−4 ns range compared to the R_2 and NOE.

Further analysis of simulated pico- to nanosecond time scale main-chain dynamics of RAP80-tUIM at 25 °C using the iRED approach[22] indicates that the N- and C-terminal helices are flexible with respect to each other (Figure 9 and Figure S1 in Supporting Information), given that the interhelical region is flexible. In addition, we have not detected long-range contacts (^{1}H−^{1}H NOEs) between residues in the different UIMs. These results immediately suggest that multivalent effects are not maximized for the UIM−polyUb recognition motif, as this would require the binding partners to be rigid, minimizing the entropic costs of binding. However, the temperature dependence of the $^{13}C_\alpha$ chemical shifts and main-chain ^{15}N relaxation data suggest that the linker is not completely flexible or completely random coil (Figures 8 and 9). Thus, while RAP80-tUIM does not maximize affinity by maintaining a binding-competent orientation for the UIM domains in the unbound state, which would compensate the entropic penalty of binding, the maximum entropic cost is not incurred either, as the linker region appears

(31) Hammes, G. G.; Chang, Y. C.; Oas, T. G. *Proc. Natl. Acad. Sci. U.S.A.* **2009**, *106*, 13737–13741.
(32) Henzler-Wildman, K.; Kern, D. *Nature* **2007**, *450*, 964–972.
(33) Spyracopoulos, L. *Protein Pept. Lett.* **2005**, *12*, 235–240.
(34) Jarymowycz, V. A.; Stone, M. J. *Chem. Rev.* **2006**, *106*, 1624–1671.
(35) Mittermaier, A. K.; Kay, L. E. *Trends Biochem. Sci.* **2009**, *34*, 601–611.
(36) Tong, Y.; Ji, C. G.; Mei, Y.; Zhang, J. Z. H. *J. Am. Chem. Soc.* **2009**, *131*, 8636–8641.

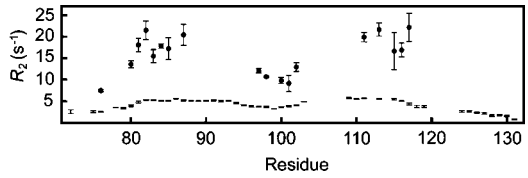

Figure 10. ^{15}N-R_2 values for RAP80-tUIM free (bars) and bound to tandem Ub_2 (circles). The baseline ^{15}N-R_2 value is indicative of the overall tumbling of the main chain (UIM helix); decreases below baseline values indicate regions of increased flexibility. Due to the low concentration and the concomitant low signal-to-noise ratio of the RAP80-tUIM sample (~120 μM), it was not possible to obtain accurate R_2 values for approximately two-thirds of the residues within the bound state; these data were excluded.

partly structured, presumably α-helical, as observed in the bound state (Figure 3c). For example, the temperature dependence of the random coil $^{13}C_\alpha$ chemical shifts in the linker region of RAP80-tUIM (Figure 8a) is indicative of structural transitions within this region, most likely between random coil and α-helix. This is consistent with the ^{15}N-R_1, R_2, and NOE NMR relaxation parameters for RAP80-tUIM (Figure 9), which indicate that the linker region is not completely flexible, or at least not as flexible as the N- and C-termini, having values between the extreme terminal regions and the partly (70% at 25 °C) α-helical UIM domains. As discussed above, the fact that only a fraction of the UIMs from RAP80 are in the α-helical conformation is an important factor underlying the strength of the UIM−Ub interaction. The entropic cost of binding can be expected to be lower than that for Ub binding to an unstructured peptide that subsequently becomes α-helical. However, this affinity gain is offset by conformational selection, or the fact that the fraction of helix is 50% at physiological temperature (37 °C).

^{15}N main-chain dynamics measurements for RAP80-tUIM indicate that the linker region between UIMs is partly flexible in free and tandem Ub_2-bound RAP80-tUIM (Figure 10). The flexibility of the linker allows the UIMs to interact with rigid monoUb moieties that are linked through flexible tethers in polyUb. From a molecular dynamics simulation for tandem Ub_3, we estimate that the correlation time for reorientation of Ub moieties with respect to each other in Ub_3 is ~15 ns (Figure S2 in Supporting Information). Considering the close structural similarity between tandem and Lys63-linked polyUb chains,[24] the inter-Ub flexibility observed in the simulation is consistent with previous NMR and small-angle X-ray scattering (SAXS) studies, which indicate that Lys63-linked chains are extended and lack interUb contacts.[37,38] In addition, NMR relaxation measurements indicate that individual Ub moieties in Lys-48-linked Ub_2 reorient on a ~10 ns time scale.[39] For RAP80, iRED analysis of the ^{15}N relaxation data indicates that N- and C-terminal UIMs reorient with respect to each other on a time scale <10 ns. With respect to a molecular mechanism for binding, specific selection of polyUb conformations by tandem UIMs can be expected to have a smaller impact on binding than conformational selection arising from the UIM helix−coil transition. For example, the initial binding of one UIM to one Ub moiety can be followed by rapid, nanosecond time scale reorientation and subsequent binding of the neighboring UIM to the neighboring Ub.

There are important consequences regarding nanosecond time scale interhelical flexibility for the UIMs and inter-Ub flexibility for polyUb chains. To reiterate the previous discussion, it is possible to maximize multivalent affinity in biological systems by employing a rigid scaffold such that tandem UIM and Ub moieties are properly positioned to minimize the entropic cost of binding. However, the flexibility between domains in both RAP80-tUIM and polyUb indicates that this plays a partial role in the molecular basis for recognition. On the other hand, the entropic penalty incurred through immobilizing adjacent UIM/Ub domains upon binding is not fully realized, as the linker between UIM domains in RAP80 appears partly structured in the unbound state (Figures 8a and 9). This has important implications for an induced-fit mechanism, where binding and stabilization of the α-helical structure of one UIM to one Ub moiety in tandem Ub_2 can lead to a cooperative structuring of the second UIM α-helix through the linker, which subsequently induces binding to the adjacent Ub moiety.

The structure of RAP80-tUIM bound to K63-linked Ub_2 (Figure 3c, PDB ID 3A1Q)[11] shows that the linker is in a helical conformation. However, the average C_α *B*-factor for the α-helices from the two molecules of RAP80-tUIM in the asymmetric unit is 22 Å^2, and this value increases to 30 Å^2 for the linker region. These results indicate that there is disorder and/or flexibility within the linker region of RAP80-tUIM in the fully bound conformation, consistent with the flexibility in the bound state as demonstrated herein by NMR relaxation measurements (Figure 10). However, given that the underlying contributions to the *B*-factor are multifaceted, there is not a quantitative relationship between *B*-factors and flexibility as measured by NMR relaxation. The NMR results presented herein and the *B*-factors from the crystallographically determined structure suggest that the linker undergoes fluctuations between unstructured and α-helical states when bound to Ub_2. This is consistent with the relatively small chemical shift changes observed for the UIM linker in RAP80-tUIM upon binding tandem Ub_2, Ub_3, and Ub_4 (Figure 3b), which indicate that while a structural change, or a shift toward a more structured state, occurs within the linker region, it does not become a rigid α-helix. These results suggest that the entropic cost of structuring the linker in RAP80-tUIM is not maximized upon binding Ub_2. Furthermore, the apparent propensity for α-helical structure within the linker region of RAP80-tUIM in the unbound state suggests that an induced-fit mechanism may be possible upon binding Ub_2.

Conclusions

The fundamental question with respect to physiology is why do Ub signaling networks utilize numerous weak ligand−Ub interactions, as opposed to tighter recognition of the Ub receptor? The answer is perhaps 2-fold:[40] first, weak binding is likely necessary for desensitization and integration of Ub signaling, because Ub must be recycled back into the free monoUb pool. If specificity and affinity were achieved by strong binding interactions, bound Ub would require removal from the cell, with subsequent up-regulation of Ub expression to replenish the free pool. Second, it is generally believed that weak binding is necessary to maintain protein interaction networks. With

(37) Tenno, T.; Fujiwara, K.; Tochio, H.; Iwai, K.; Morita, E. H.; Hayashi, H.; Murata, S.; Hiroaki, H.; Sato, M.; Tanaka, K.; Shirakawa, M. *Genes Cells* **2004**, *9*, 865–875.
(38) Varadan, R.; Assfalg, N.; Haririnia, A.; Raasi, S.; Pickart, C.; Fushman, D. *J. Biol. Chem.* **2004**, *279*, 7055–7063.
(39) Ryabov, Y.; Fushman, D. *Proteins: Struct., Funct., Bioinf.* **2006**, *63*, 787–796.
(40) Hicke, L.; Schubert, H. L.; Hill, C. P. *Nat. Rev. Mol. Cell Biol.* **2005**, *6*, 610–621.

respect to K63 polyUb signaling in the DDR pathway, high-resolution imaging of DNA double-strand break foci indicates a remarkable degree of plasticity within these structures; not only do they rapidly form after the initial genotoxic stress, but they also reorganize as evidenced by changes in size and number of foci following damage.[41] Our results show that the recognition of polyUb by RAP80 is dynamic, providing a flexible mechanism for the transient initiation of DNA damage foci that ultimately regulate DNA repair.

Acknowledgment. This research was funded by Canadian Institutes of Health Research (CIHR), the Alberta Heritage Foundation for Medical Research (AHFMR), and the University of Alberta. We thank Junjie Chen for providing RAP80 cDNA, Pascal Mercier for assistance with programming, J. N. Mark Glover for critical reading of the manuscript, and the Canadian National High Field NMR Centre (NANUC) for assistance and for use of the facilities. Operation of NANUC is funded by the Natural Science and Engineering Research Council of Canada and by the University of Alberta. Computational studies were enabled by the use of computing resources provided by WestGrid and Compute/Calcul Canada. L.S. is an AHFMR Senior Scholar.

Supporting Information Available: Two figures showing ^{15}N-R_1, R_2, and $\{^1H\}-^{15}N$ NOE values for RAP80-tUIM and time correlation functions for interUb vectors from tandem Ub_3; detailed descriptions of the models describing multivalent binding between RAP80−tUIM and tandem polyUb chains; protein sequences for RAP80-tUIM, Ub, and tandem Ub_2, Ub_3, and Ub_4 polyUb chains; and complete ref 21. This material is available free of charge via the Internet at http://pubs.acs.org.

JA103869X

(41) Aten, J. A.; Stap, J.; Krawczyk, P. M.; van Oven, C. H.; Hoebe, R. A.; Essers, J.; Kanaar, R. *Science* **2004**, *303*, 92–95.